International Journal of Pharmaceutics 423 (2012) 440–451

Contents lists available at SciVerse ScienceDirect

International Journal of Pharmaceutics

journal homepage: www.elsevier.com/locate/ijpharm

Pharmaceutical nanotechnology

Physicochemical characterization of curcuminoid-loaded solid lipid nanoparticles

Andreas Noack[a], Gerd Hause[b], Karsten Mäder[a,*]

[a] Insitute of Pharmacy, Martin Luther University Halle-Wittenberg, Wolfgang-Langenbeck-Straße 4, 06120 Halle, Saale, Germany
[b] Microscopy Unit, Martin Luther University Halle-Wittenberg, Weinbergweg 22, 06120 Halle, Saale, Germany

ARTICLE INFO

Article history:
Received 19 September 2011
Received in revised form 6 December 2011
Accepted 8 December 2011
Available online 16 December 2011

Keywords:
Nanoparticles
SLN
Curcumin
High pressure homogenization
Raman spectroscopy
Fluorescence

ABSTRACT

Curcuminoid-loaded solid lipid nanoparticles (SLN) were produced by melt-homogenization. The used lipid matrices were medium chain triglycerides, trimyristin and tristearin. The resulting nanoparticles had an anisometric shape and a platelet-like structure. Curcuminoid-loaded trimyristin particles did not solidify when stored at room temperature. The supercooled state of trimyristin was studied by DSC and ^{1}H NMR experiments. A partial recrystallization of the lipid matrix was detected but no change of the mobility of the lipid was noted. Nanoparticles based on tristearin had an α- and β-modification which was subsequently converted into the stable β-phase. Curcuminoids did neither influence the melting behavior nor the crystalline or geometric structure of the particles. The interactions between the curcuminoids and the lipid matrix were investigated by Raman and fluorescence spectroscopy. The shape of the curcuminoid bands in the Raman spectra suggested that the drug was in an amorphous state. The fluorescence spectra showed an effect of the lipid matrix on fluorescence properties of the curcuminoids. It was further demonstrated that the drug was not secluded by the solid lipid matrix, but it was influenced by the surrounding aqueous environment. Fluorescence anisotropy measurements revealed a decreased mobility of the curcuminoids within the nanodispersions. From the results of Raman and fluorescence measurements it was concluded that the drug was mainly located on the surface of the crystalline particles.

1. Introduction

Turmeric (*Curcuma longa* L.) is a commonly cultivated plant in south and south-east Asia. Its rhizome has been used in traditional Indian medicine for many years. The polyphenol curcumin (diferuloylmethane) is the major ingredient of the rhizome of turmeric and responsible for its intensive yellow color. Curcumin is in the focus of biomedical and pharmaceutical research for many years and numerous articles reported of its manifold effects (Aggarwal et al., 2006; Anand et al., 2008a,b). It was published that curcumin mainly interacts with various mediators of the inflammatory cell response and leads to a suppression of these factors (Aggarwal and Harikumar, 2009; Zhong et al., 2011). It is therefore seen as a valuable drug for the treatment of different diseases. Among others, the potential activity of curcumin against cancerous diseases has been studied intensively in the last decade (Youssef and El-Sherbeny, 2005; Duvoix et al., 2005; Strimpakos and Sharma, 2008; Tuli et al., 2011). The major drawback of curcumin is its very low bioavailability after oral application which is caused by a poor solubility in aqueous media and its rapid metabolism within the intestine (Anand et al., 2007). Lao et al. (2006) detected only nanomolar concentrations of curcumin in the blood of humans after the application of the large dose of 12 g of drug. Hence, there is a clear need to improve the bioavailability of this substance to verify the high expectations which were placed in curcumin in the past years.

Since almost 20 years solid lipid nanoparticles (SLN) were investigated as potential drug delivery systems (Müller et al., 1995). Major advantages of these systems are the high biocompatibility, the avoidance of organic solvents during production and the easy scale up of the fabrication (Mehnert and Mäder, 2001). SLN have been intensively tested for oral delivery of drugs and were reported to increase the bioavailability of the incorporated drugs (Yang et al., 1999; Priano et al., 2007). However, the physicochemical characteristics of the lipid particles must be taken into account (Mehnert and Mäder, 2001). The lipid polymorphism, the coexistence of other colloidal structures and the interaction of drug and matrix are of particular interest. Therefore, a broad spectrum of analytical techniques is needed to gather information about the aforementioned properties. Scope of this paper was a

Abbreviations: MCT, medium chain triglycerides; MCT-NE, MCT nanoemulsion; TM, trimyristin; TM-NE, trimyristin particles supercooled melt; TM-NS, trimyristin particles crystalline form; TS, tristearin; TS-NS, tristearin particles; TMCurc-NE, curcuminoid-loaded preparation.

* Corresponding author at: Martin Luther University Halle-Wittenberg, Department of Pharmaceutical Technology and Biopharmaceutics, Wolfgang-Langenbeck-Str. 4, 06120 Halle, Saale, Germany. Tel.: +49 345 5525167; fax: +49 345 5527029.
E-mail address: karsten.maeder@pharmazie.uni-halle.de (K. Mäder).

0378-5173/$ – see front matter © 2012 Elsevier B.V. All rights reserved.
doi:10.1016/j.ijpharm.2011.12.011

detailed physicochemical characterization of curcuminoid-loaded lipid nanodispersions. The melting behavior and polymorphism of the lipid matrix were investigated by DSC. ^{1}H NMR provided information about the mobility of the lipid phase and the emulsifier. The shape of the solid lipid particles was revealed by electron microscopy. A closer insight in the interaction between drug and lipid matrix was gained by Raman spectroscopy and fluorescence spectroscopy. The localization of the curcuminoids within the particles and their physical state were the main objectives for the application of these techniques. Furthermore, the mobility of the drug in the nanodispersions was assessed by fluorescence anisotropy measurements.

2. Materials and methods

2.1. Materials

The following substances were used: curcuminoids (mixture of curcumin, desmethoxycurcumin, bisdesmethoxycurcumin, content ≥95.0%, Fluka, Switzerland), medium chain triglycerides (MCT, Miglyol® 812, Caelo, Germany), trimyristin (TM, Dynasan 114, Sasol, Germany), tristearin (TS, Dynasan 118, Sasol, Germany), poloxamer 188 (Lutrol® F68, BASF, Germany). All other used chemicals were at least of reagent grade.

2.2. Methods

2.2.1. Preparation of nanodispersions

The lipid nanodispersions were produced by high pressure homogenization. The lipid phase, consisting of MCT, TM or TS, was coarsely emulsified in the water phase by a high speed dispersion device. This pre-emulsion was further processed with a high pressure homogenizer (Blümer and Mäder, 2005). The lipid concentration in the dispersions was 10% (w/w) and the formulations were either prepared drug-free or loaded with 0.1% (w/w) curcuminoids if not stated otherwise.

Generally, the lipid phase was heated to a temperature of 70–85 °C. The curcuminoids were dissolved in the hot and molten lipid phase. Thereafter, a preheated aqueous solution of 2.5% (w/v) poloxamer 188 and 0.05% (w/v) sodium azide was added to the lipid phase. A pre-emulsion was formed by using an ultra turrax (IKA, Staufen) at 14,000 rpm for 5 min. The resulting dispersion was further homogenized in a nine cycle homogenizing regime, using a two stage high pressure homogenizer (Stansted Fluid Power Ltd.). For the first three cycles the main pressure was set at 50 MPa. The pressure was increased every three cycles to 70 MPa and 100 MPa respectively. The second stage pressure was constantly kept at 10 MPa during the whole procedure. The homogenizer was also heated up with a water bath to 75 °C avoid recrystallization of the high-melting lipids and to decrease the viscosity of the lipids. The hot dispersion was given through a 0.8 μm cellulose acetate filter. The formulation was cooled down slowly to room temperature and stored in glass vessels at 8 °C if not declared otherwise. To avoid photolytical decomposition of the curcuminoids the samples were kept protected from light.

2.2.2. Determination of particle size

Laser diffraction (LD, Mastersizer, Malvern, UK) was applied routinely to measure the particle size shortly after preparation. The samples were analyzed in quintuplicate. The volume weighted size distribution was calculated by applying the Mie theory. A refractive index of 1.45 was assumed. The d_{10}, d_{50} (median), the volume weighted mean and the d_{90} were used for the evaluation of the particle size. Photon correlation spectroscopy (PCS, HPPS, Malvern, UK) was additionally carried out for the determination of the particle size distribution. The dispersions were adequately diluted with bidistilled water and measured in triplicate. The *z*-average and the PDI were applied for the evaluation of the particle size. The dispersions were further examined with a light microscope (Axiolab, Zeiss, Germany) with non-polarized light and with polarized light.

2.2.3. Differential scanning calorimetry (DSC)

Calorimetric measurements were performed by a Netzsch DSC 200 apparatus (Netzsch, Germany). Samples were accurately weighed in dotted aluminum pans (approximately 15 mg). Nitrogen was used as flush gas. The scans were recorded with a heating rate of 5 K/min for the bulk lipid and 2 K/min for the nanodispersions, if not stated otherwise. The respective cooling rate was 10 K/min and 5 K/min for the preparations. Besides constant heating some samples were also heated discontinuously by bringing the dispersions to 40 °C, holding this temperature for 1 h and subsequently heating them to 80 °C.

2.2.4. X-ray scattering

The patterns of the TM and TS bulk material and the patterns of the TM-NE, TM-NS and TS-NS preparations were recorded in transmission with a stationary linear position sensitive detector (2θ = 0–40°) on a stage including a curved primary Ge (1 1 1) monochromator and high temperature attachment (STOE & CIE GmbH, Germany). The samples were sealed into glass capillaries. Cu Kα1 radiation was used and the scattering pattern of the powder samples was corrected with respect to an empty capillary and the pattern of the nanodispersions was corrected with respect to a capillary filled with distilled water. The resulting patterns were combined in one diagram to present both SAXS and WAXS region (2θ = 0–40°, s = 0–4.7 nm^{-1}) (Förster et al., 2007).

2.2.5. Transmission electron microscopy (TEM)

The shape and the size of every produced dispersion were investigated by electron microscopy. Negatively stained samples were prepared by spreading 3 μl of the dispersion onto a Cu grid coated with a formvar film. After 1 min of adsorption, excess liquid was blotted off with filter paper. After washing with water (3 times for 1 min) the grids were placed on a droplet of 1% aqueous uranyl acetate and drained off after 1 min. The dried specimens were examined with a EM 900 transmission electron microscope (Zeiss, Germany) at an acceleration voltage of 80 kV. Electron micrographs were taken with a Variospeed SSCCD camera SM-1k-120 (TRS, Germany).

For freeze fracture, the lipid nanodispersions were freeze fixed using a propane jet-freeze device JFD 030 (BAL-TEC, Balzers, Liechtenstein). Thereafter the samples were freeze-fractured at −150 °C without etching with a freeze fracture/freeze etching system BAF 060 (BAL-TEC, Balzers, Liechtenstein). The surfaces were shadowed with platinum to achieve a good topographic contrast (2 nm layer, shadowing angle 45°) and subsequently with carbon to stabilize the ultra-thin metal film (20 nm layer, shadowing angle 90°). The replicas were floated in sodium chloride (4% NaCl; Roth, Karlsruhe, Germany) for 30 min, rinsed in distilled water (10 min), washed in 30% acetone (Roth, Karlsruhe, Germany) for 30 min and rinsed again in distilled water (10 min). Thereafter the replicas were mounted on copper grids coated with formvar film and observed with a transmission electron microscope.

2.2.6. Nuclear magnetic resonance spectroscopy (NMR)

800 μl of the respective formulation was mixed with 200 μl D_2O containing 0.75% (v/v) of sodium 3-(trimethylsilyl)-2,2,3,3-d_4 propionate as internal standard. ^{1}H NMR was performed at a temperature of 27 °C and a frequency of 400 MHz with a Gemini 2000 (Varian, France).

2.2.7. Raman spectroscopy

The Raman spectra were recorded by a Fourier transform Raman spectrometer RFS 100/S (Bruker, Germany). The solid bulk materials were brought into the cavity of an aluminum pan. Liquid samples were placed in glass tubes. The excitation source was a diode pumped Nd:YAG laser operating at a wavelength of 1064 nm. Spectra were detected at an angle of 180° relative to the incident beam. Every sample was analyzed with 200 scans at a laser power of 350 mW. The spectra were processed by the Bruker OPUS software (Jores et al., 2005).

The temperature dependence of the spectra of the TMCurc-NE and TMCurc-NS preparations was investigated in the range from 0 °C to 70 °C. After each temperature adjustment, the temperature was equilibrated for 10 min and subsequently the spectra were recorded.

2.2.8. Fluorescence spectroscopy

Fluorescence measurements were accomplished by a Hitachi F-4500 spectrophotometer (Hitachi Ltd., Japan). A xenon lamp was used as the light source. The excitation wavelength was set to 420 nm and the spectra were recorded in a range of 430–620 nm. The width of the slit was 5 nm and the speed of the scan was set to 60 nm/min. The fluorescence intensity was measured in an angle of 90°. The cuvette holder was connected to a thermostat to set the desired temperature during measurement.

Polarized light was generated by inserting a polarization filter (Hitachi Ltd., Japan) into the incoming light path. A second polarization filter was placed in front of the light detector. The polarization filters were moved into appropriate parallel and perpendicular position. The excitation wavelength was set to 430 nm and the recorded range was 470–540 nm for the experiments with polarized light. The scan speed was reduced to 15 nm/min for these experiments. The steady-state anisotropy r is defined as

$$\langle r \rangle = \frac{(I_{\parallel} - GI_{\perp})}{(I_{\parallel} + 2GI_{\perp})} \quad (1)$$

$I_{\parallel}$ is the fluorescence intensity parallel to the excitation polarization and $I_{\perp}$ is the fluorescence intensity perpendicular to excitation polarization (Lakowicz and Masters, 2008). G is a factor which corrects the bias of the detection system on the emitted polarized light and is obtained by

$$G = \frac{I_{hv}}{I_{hh}} \quad (2)$$

$I_{\parallel}$ and $I_{\perp}$ of the curcuminoid-loaded nanoparticles were corrected for light scattering by subtracting a background spectrum of a curcuminoid-free dispersion.

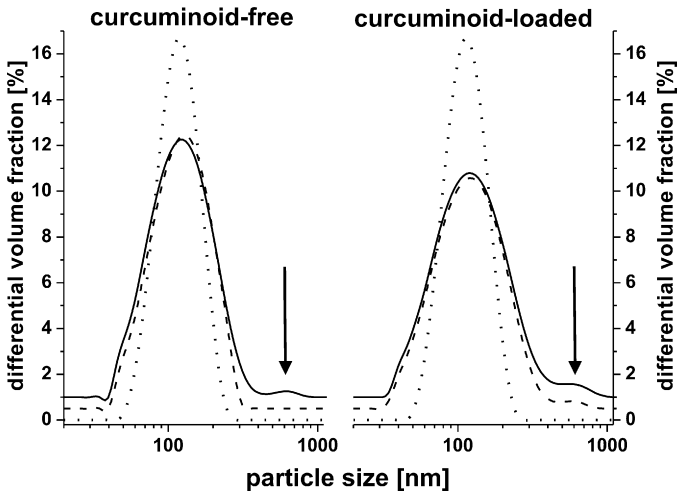

Fig. 1. Distribution curves recorded by laser diffraction of samples of MCT-NE and MCTCurc-NE (···), TM-NE and TMCurc-NE (- - -), TM-NS and TMCurc-NS (—). The distribution curves were shifted along the ordinate for better visualization. The arrows highlight the fraction of particles >500 nm.

3. Results and discussion

3.1. Particle size distribution

The MCT-NE dispersions had a small and narrow size distribution (Fig. 1). The mean particle size was found to be approximately 130 nm. The TM dispersions exhibited mean particle sizes of up to 161 nm and had a broader distribution compared to MCT. The particle size distributions of the TS preparations were similar to the TM formulations. The d_{90} was below 300 nm for every formulation (Table 1). Besides the broader main peak the TM and TS dispersions also showed a small side peak between 600 and 800 nm (Fig. 1, arrow). The investigation of these dispersions in a light microscope revealed no particles bigger than 1 μm. The z-average diameters of MCT-NE and MCTCurc-NE were 130 and 137 nm respectively and the PDI was 0.07. The respective mean values of PCS and LD were in good agreement for these samples which pointed to a narrow and monomodal size distribution of the MCT based dispersions. The other formulations exhibited z-average diameters in the range of 153–205 nm with a PDI below 0.12. The side peak of the TM and the TS dispersions which was detected by LD was not found with PCS. The calculated mean diameters of the PCS and LD measurements differed distinctly for these dispersions (Table 1). Generally, the z-average diameter estimated by PCS tended to be higher compared to the mean diameter estimated by LD. It was concluded that the aforementioned side fraction between 600 and 800 nm of the TM and TS formulations were causing the discrepancies between the applied particle sizing techniques. Furthermore, the

Table 1
Particle size distribution of the formulations determined by dynamic and static light scattering.

Sample	PCS		LD			
	z-Av. (nm)	PDI	d 0.1 (nm)	Median (nm)	Mean (nm)	d 0.9 (nm)
MCT-NE[a]	137.7 ± 0.6	0.07	83	125	130	185
MCTCurc-NE[b]	130.0 ± 1.7	0.07	80	120	126	179
TM-NE[a]	153.7 ± 0.6	0.1	73	130	139	220
TMCurc-NE[b]	165.0 ± 0	0.1	67	132	152	258
TM-NS[a]	170.7 ± 0.6	0.12	71	130	146	235
TMCurc-NS[b]	185.0 ± 1.0	0.12	66	130	157	266
TS-NS[a]	194.3 ± 1.5	0.07	75	140	156	246
TSCurc-NS[b]	205.0 ± 1.0	0.11	69	137	161	267

[a] Composition: 10% lipid (w/w), 2.5% poloxamer 188 (w/w).
[b] Composition: 10% lipid (w/w), 2.5% poloxamer 188 (w/w), 0.05–0.1% curcumin (w/w).

anisometric shape of the particles in the crystalline suspensions (TM-NS and TS-NS) must be taken into account as well (see Section 3.4). One should keep in mind that it remains difficult for light scattering techniques, like PCS and LD to describe the size of non-spherical particles properly. In contrast to a sphere, the size of an anisometric particle cannot be described with one single size parameter, like the diameter, because the dimensions of anisometric particles are different in the respective spatial orientation. The applicability of the light scattering techniques and the correct interpretation of the gained results was discussed in the literature recently (Nobbmann and Morfesis, 2009; Kuntsche et al., 2009).

In summary, the evaluation of a particle size distribution strongly depends on the applied method and on the properties of the examined particles. However, it is vital that the applied particle measuring technique is capable of detecting fractions of larger particles (>700 nm), because these particles may influence the stability of the dispersion. The prepared TM and TS dispersions showed a broad distribution and a distinct particle fraction bigger than 700 nm. Therefore, the LD measurements should be seen as more applicable for the evaluation of the particle size distribution TMCurc-NS and TSCurc-NS, because fractions of particles >700 nm are estimated more reliable with this technique. A determination of the particle size distribution solely with PCS measurements was seen as insufficient for the characterization of the formulations.

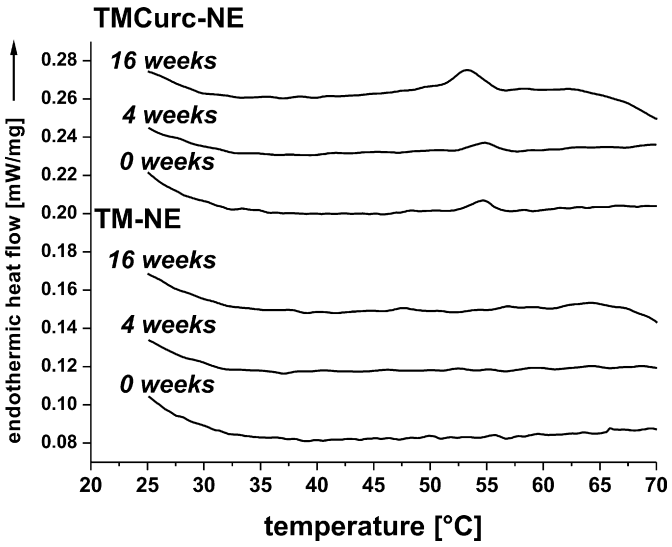

Fig. 2. DSC thermograms of the heating curves of TM-NE and TMCurc-NE samples. The DSC scans were recorded a few hours, 4 weeks and 16 weeks after preparation and storage at 22 °C. The thermograms were shifted along the ordinate for better visualization.

3.2. DSC

The melting and the recrystallization point of the TM and TS nanoparticles were lower compared to the bulk material. The melting points of the bulk material were found to be 58 °C for TM and 72 °C for TS. Lutton (1945) published approximately the same melting points for these triglycerides. The TM nanodispersions had a melting point of 54 °C and the TS preparations were melting at 68 °C. As Bunjes et al. (2000) reported earlier, the shift of the melting peaks can be explained by the colloidal nature of the samples. Despite the melting point depression, it was concluded that TM and TS existed in β-modification within the particles. Additionally, the melting peaks of the nanoparticles were broader than the peaks of the raw materials. The size-dependent melting of the particles is seen as the underlying reason for this observation. The existence of different particle fractions in the investigated samples was confirmed by the light scattering experiments and by the TEM-micrographs (see corresponding sections).

The crystallization point of the preparations was shifted dramatically to lower temperatures. The molten particles did solidify around 15 °C below the crystallization point of the bulk lipid. This shift must not be seen as absolute, because crystallization is a complex process which is influenced by a variety of parameters. Nevertheless, it shows that a small particle size is one key parameter for the delay of the lipid crystallization. The big depression of the crystallization point resulted in a non-solidification of the curcuminoid-loaded TM particles when cooled down to 22 °C after production (Fig. 2). The occurrence of supercooling behavior was reported for several formulations of lipid nanodispersions (Westesen and Bunjes, 1995). This effect made it possible to investigate the lipid either in the crystalline or in the liquid state. The DSC curves of the TM particles, stored at 22 °C showed no melting event during the observation period of 16 weeks. In several curcuminoid-loaded preparations a minor melting event at 54–55 °C was detected (Fig. 2). Hence, a small fraction of lipid was crystallized in these samples. The peak was getting more pronounced over 16 weeks. The observed behavior of the curcuminoid loaded TM formulations emphasized the metastable character of supercooled lipid nanoparticles. The presence of the curcuminoids seemed to induce crystallization of the lipid matrix. It was suggested that the drug precipitated after the production in the cold lipid matrix. The precipitated curcuminoids might, in turn, induce the partial solidification of the lipid carrier.

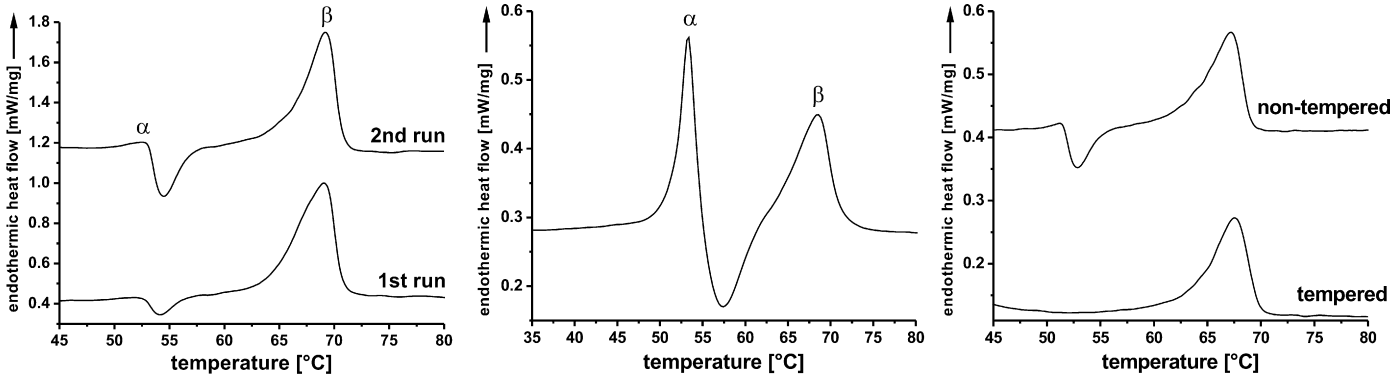

Fig. 3. DSC thermograms of: (A) two consecutive heating runs of a TSCurc. NS dispersion with an intermediate cooling step (not shown). Greek letters indicate the melting point of the respective modification, (B) heating curve (5 K/min) of a TSCurc-NS dispersion recorded after previous melting and subsequent rapid cooling (10 K/min, scans not shown), (C) heating curves of two TSCurc-NS dispersions after melting and subsequent cooling (scans not shown). Non-tempered sample: continuous heating. Tempered sample: discontinuous heating. The thermograms were shifted along the ordinate for better visualization.

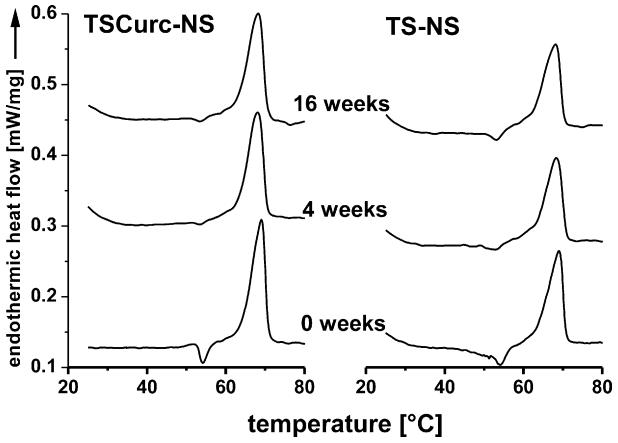

Fig. 4. DSC thermograms of the heating curves of samples of TSCurc-NS and TS-NS. The DSC scans were recorded a few hours, 4 weeks and 16 weeks after preparation and storage at 22 °C. The thermograms were shifted along the ordinate for better visualization.

Crystalline TM particles were only obtained when the formulation was cooled down to 8 °C. Under these conditions, the TM particles transformed rapidly into the β-modification so that the unstable, intermediate α- or β′-modifications were not detected. The melting enthalpy was determined to 19 J/g, being about 10% of the enthalpy of the bulk lipid. The content of lipid in the dispersions was 10% (w/w). It was therefore concluded that the TM matrix did crystallize completely.

Freshly prepared TS nanoparticles showed an exothermal peak at around 55 °C additionally to the melting of the β-modification at 68 °C (Fig. 3A). The small endothermal peak and the subsequent exothermal peak were related to the melting of the α-lipid modification and the subsequent crystallization in the β-modification. Comparable results have been reported for nanoparticles consisting of pure triglycerides (Bunjes et al., 2007). The transition was getting even more intense if the samples were heated a second time after previous cooling (Fig. 3A). A higher cooling rate was further enforcing the formation of the α-phase in the TS particles (Fig. 3B). Unprocessed TS exhibited the same behavior as the nanoparticles. The α-fraction of the TS nanoparticles was decreasing over the observation period of 16 weeks (Fig. 4). Tempering of the sample at a temperature close to the melting point of the α-modification resulted in a fast ordering of the lipid crystals to the β-modification without any detectable residues of the α-phase (Fig. 3C). The melting enthalpy of the TS nanoparticles in β-modification was 21.6 J/g, being almost 10% of the respective bulk enthalpy. Hence, the lipid matrix in the TS nanodispersions was concluded to fully crystallize, as well.

The comparison of the drug-free and the curcuminoid-loaded lipid nanodispersions revealed no influence of the drug on the melting behavior. The presence of curcuminoids did not have any impact on the occurrence or the sequence of the phase transition of the lipids during solidification.

At least for pure triglyceride matrices the supercooled state is concluded to be not suitable as a drug carrier, because uncontrolled recrystallization can take place. This may result in drug expulsion from the particles or other unpredictable effects. However, for other lipid systems more stable supercooled preparations have been described (Kuntsche et al., 2004).

In accordance with the results of Bunjes et al. (1996) the ordering of the TM chains during recrystallization was very fast, so that the unstable α-phase was not verifiable in these dispersions under the applied experimental conditions. In contrast, the solidification of the TS melt takes place in part via the α-modification, because the chain ordering process to a stable modification is slower due to the higher chain length. It was shown that this transition was accelerated when the sample is stored at higher temperatures, e.g. 40 °C for a short time.

3.3. X-ray scattering

The crystalline modification of the lipid matrix was elucidated in more detail with X-ray scattering. The small angle and wide angle area and the respective reflexes were recorded simultaneously. The supercooled TM particles showed no sharp reflexes, but two broad halos which pointed to a low long range order usually found in amorphous or fluid systems. This result confirmed that the non-solidification of the TM nanoparticles at a storage temperature of 22 °C. They remained in a metastable liquid state.

When the cold stored TM-NS and TS-NS preparations were examined, three main peaks were observed in the wide angle finger-print area at 2.2 nm^{-1}, 2.6 nm^{-1} and 2.7 nm^{-1} were observed (Fig. 5). The pattern of the bulk showed the same reflexes. The described peaks in the wide angle area are typical for a triclinic subcell occurring in the β-modification (Small and Hanahan, 1986). In agreement with the DSC measurements it was confirmed that the nanoparticles containing either TM or TS in β-modification.

The sharp single reflexes in the small angle domain further confirmed the crystalline structure of the TM-NS and TS-NS dispersions. The recorded values for the long and the short spacing and the respective literature data were summarized in Table 2.

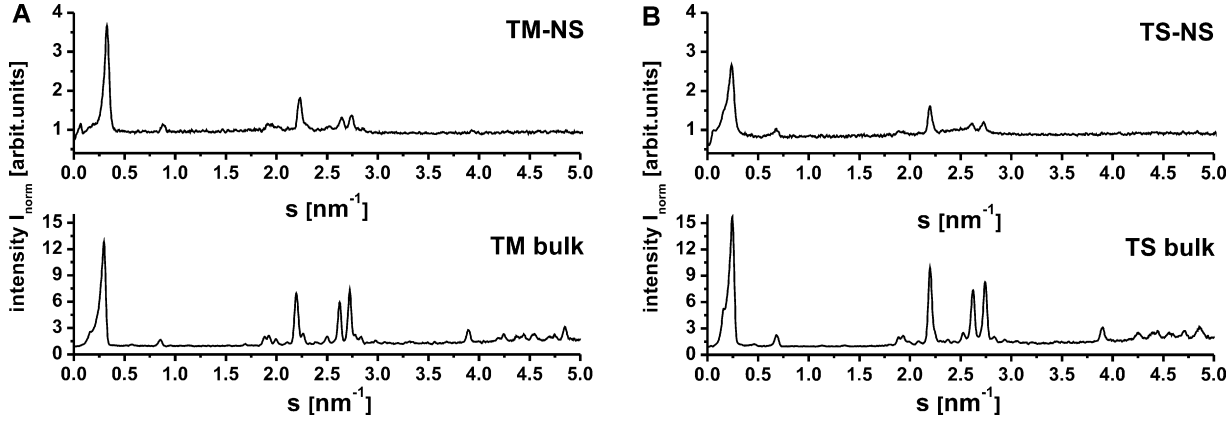

Fig. 5. X-ray diffraction pattern of (A) TM-NS nanoparticles and TM bulk and (B) TS-NS nanoparticles and TS bulk. Small and wide angle area were recorded simultaneously.

Table 2
Short and long spacings of the recorded pattern and the theoretical values of the β-modification found in the literature.

Sample	Short spacing d^a (nm)	Short spacing d (nm) β[b]	Long spacing d^a (nm)	Long spacing d (nm) β[b]
TM bulk	0.46, 0.38, 0.37	0.46, 0.38, 0.37	3.51	3.55
TM-NS SLN	0.46, 0.38, 0.37		3.44	
TS bulk	0.45, 0.38, 0.36	0.46, 0.38, 0.37	4.42	4.51
TS-NS SLN	0.45, 0.38, 0.36		4.42	

[a] d values were calculated by $d = 1/s$, s = reciprocal spacing (nm^{-1}).
[b] Data obtained from Lutton (1945).

3.4. Transmission electron microscopy (TEM)

The detailed geometry of the nanoparticles was investigated by preparing TEM micrographs. Images of the nanoemulsions prepared by the negative stain technique were exhibiting the expected round droplets (data not shown). The size of the droplets estimated in the micrographs was bigger compared to the values obtained by laser diffraction which was caused by the spreading of the droplets on the copper grid during the preparation. The solid lipid nanoparticles revealed an anisometric structure with a huge diversity in shape (Fig. 6). The observed geometries were rotund, rhombic or completely irregular. Generally, smaller particles appeared more round or oblong, whereas the bigger particles revealed a platelet structure typical for lipid particles in β-modification (Bunjes et al., 2003). From the freeze-fractured samples a lamellar structure of the lipid matrices could be suggested (Fig. 6). The overall thickness of the examined particles was between 50 and 70 nm. The thickness of one single molecular layer inside the TM and the TS particles was determined by X-ray diffraction to be 3.5 and 4.5 nm respectively. Therefore, these particles consisted of approximately fifteen single layers.

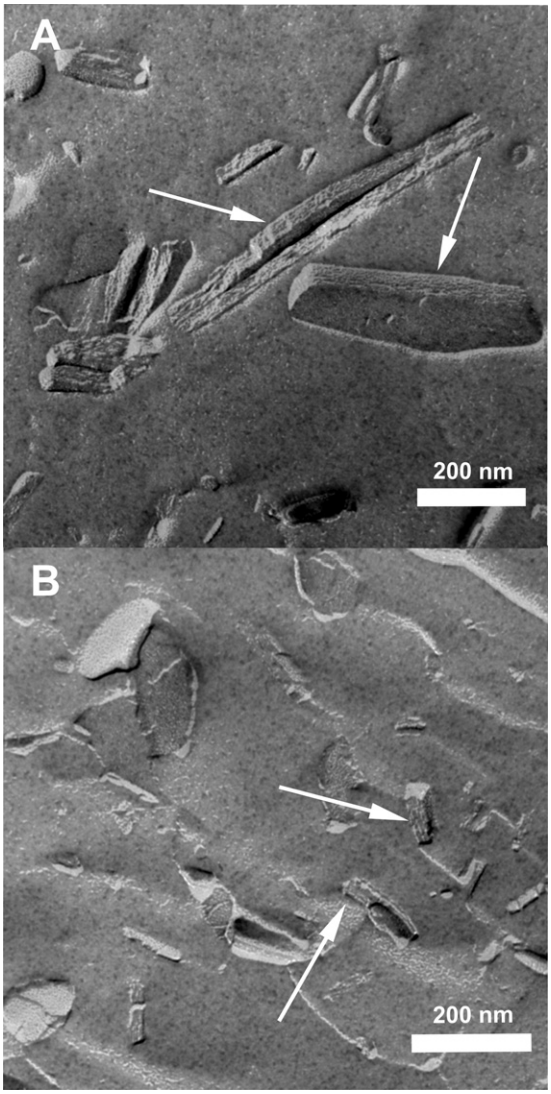

Fig. 6. TEM images of (A) a TMCurc-NS dispersion and (B) a TSCurc-NS dispersion. The arrows highlight the lamellar structure of particles with a fractured surface.

3.5. NMR

In contrast to DSC, the ^{1}H NMR experiments can be performed using constant temperature conditions. This is a special advantage for the investigation of colloidal systems, because some non-ionic surfactants are subjected to transformations, e.g. clouding or gelation under the influence of heat (Al-Saden et al., 1982). Disadvantages of standard ^{1}H NMR spectroscopy are the inaccessibility of solid materials and the comparably low sensitivity of the method. Thus, an investigation of the incorporated drug was not possible, because of its low concentration in the dispersions. With regard to the curcuminoid-loaded nanoparticles a detailed analysis of the lipid matrix and of the emulsifier was carried out.

An overview of the detected peaks and their assignment to a certain structure is given in Fig. 7. The good separation of the lipid and the emulsifier signals enabled the characterization of both compounds without interference by the other one. The spectra of the lipid nanodispersions were evaluated in terms of peak appearance and line width at the half amplitude of the respective peak. This parameter is an indicator of the mobility of the fluid component. A highly viscous or solid matrix leads to a broadening or complete disappearance of the peaks.

A comparison of the spectra of the MCTCurc-NE and TMCurc-NE preparation revealed only minor differences (Fig. 8A). The presence of the peaks a–g in the supercooled TM dispersion clearly showed the fluid state of the lipid matrix. The line width of peak f (1.6 ppm) of the TM dispersions was 10 Hz. The line width of the same peak was 13 Hz for the MCT dispersion. The line width of peak e (1.6 ppm) was approximately 20 Hz for MCTCurc-NE and TMCurc-NE. The higher intensity of peak e in TM-NE compared to MCT-NE was caused by the longer alkyl chain of the myristic acid. The line width of peak g (0.9 ppm) was not determinable because of the triplet structure. The similar peak appearance of both formulations indicated a high mobility of the fatty acid chains in the respective emulsion droplets. Therefore, the state of the lipid chains in the supercooled TM dispersions was comparable with the state of the MCT-based emulsion. The shape and the line width of the peaks of the supercooled TM preparation were not changing over an observation period of 3 weeks (Fig. 8B). Thus, the conditions in the emulsions droplets were not changing with time and no further ordering of the lipid chains was detected. The sharp poloxamer 188 peaks proved the high mobility of the emulsifier in the preparation. The poloxamer 188 duplet (1.15 ppm) was broadening within 3 weeks and the partition of the two peaks was less sharp compared to the beginning. The singlet at 3.7 ppm was also slightly

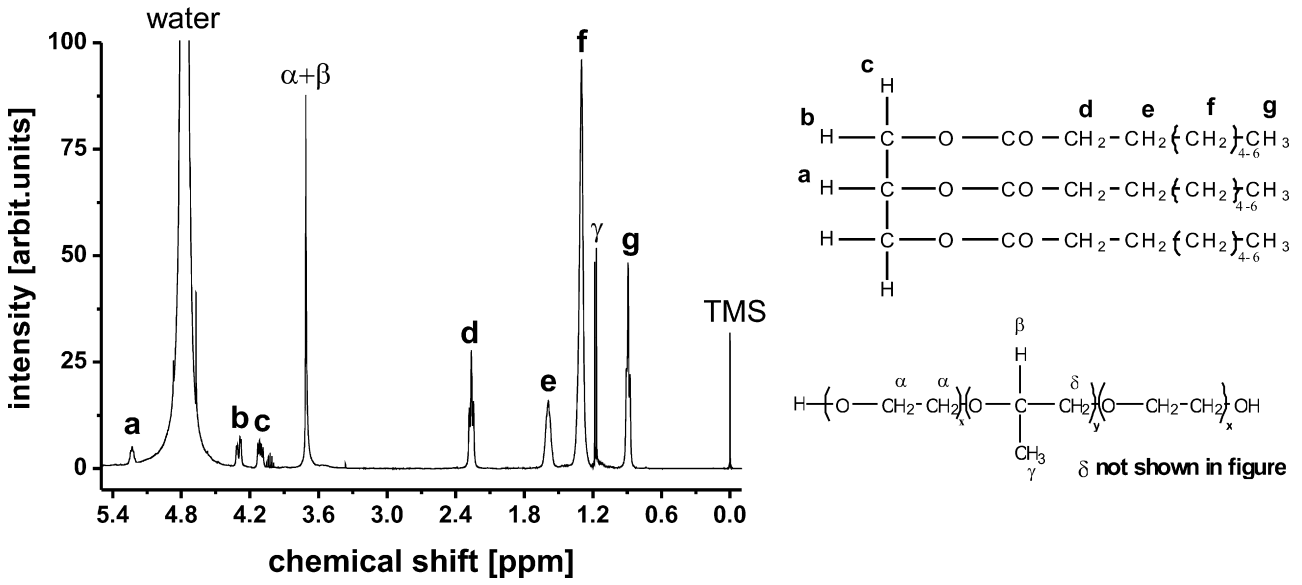

Fig. 7. [1]H NMR spectrum of a MCTCurc-NE dispersion. The Latin letters assign the signals in the NMR-spectra to the protons in the formula of a triglyceride. The Greek letters assign the signals in the NMR-spectra to the protons in the formula of poloxamer 188 (according to Jores et al., 2003).

broadening from 3 Hz to 5 Hz during the observation period. The time-dependent change of the line width was probably caused by a further ordering of the polymer chains during storage.

The spectrum of the crystalline TM nanoparticles showed signals of protons of the fatty acid chain (Fig. 9A). The detected peaks were attributed to the protons of the terminal methyl group (peak g, 0.9 ppm) and to the methylene protons belonging to the distal carbons of the fatty acid chain (peak f, 1.3 ppm, Fig. 9B). The signals a–e representing the proximal protons of the triglyceride were not detectable (Fig. 9A, for peak a–e see Fig. 7). The line width of peak f was 6–7 Hz. Thus, the protons were as mobile as in the emulsion droplets of the supercooled dispersions. Peak f was still detectable but less strong after 5 months of storage at 8 °C and its line width was not changed significantly. In contrast peak g vanished with time and could hardly be detected after 150 days (data not shown). The appearance of the mentioned peaks was unexpected, because the protons in the chains of the solid lipid matrix cannot give any signal. Hence, the remaining signals were assigned to mono- and diglycerides and free fatty acids of TM (Fig. 9B). These molecules can be inherent in the used lipid as a residue of the production process. A partial saponification during the production of the nanodispersions was also possible, because the lipid was exposed to heat and wetness over a longer period of time. Due to their increased hydrophilic properties the partial glycerides and free fatty acids were likely to be located in the interface between water and lipid phase. So these molecules were either situated on the surface of the particles or were solubilized by the emulsifier in the water phase. In contrast, the spectra of the TS dispersions revealed no peaks associated to the lipid protons (Fig. 9B). On the one hand the concentration of stearic acid and partial glycerides might have been too low to give a signal. On the other hand these substances are more lipophilic and therefore they may have crystallized together with the triglyceride instead of residing in the amphiphilic interface.

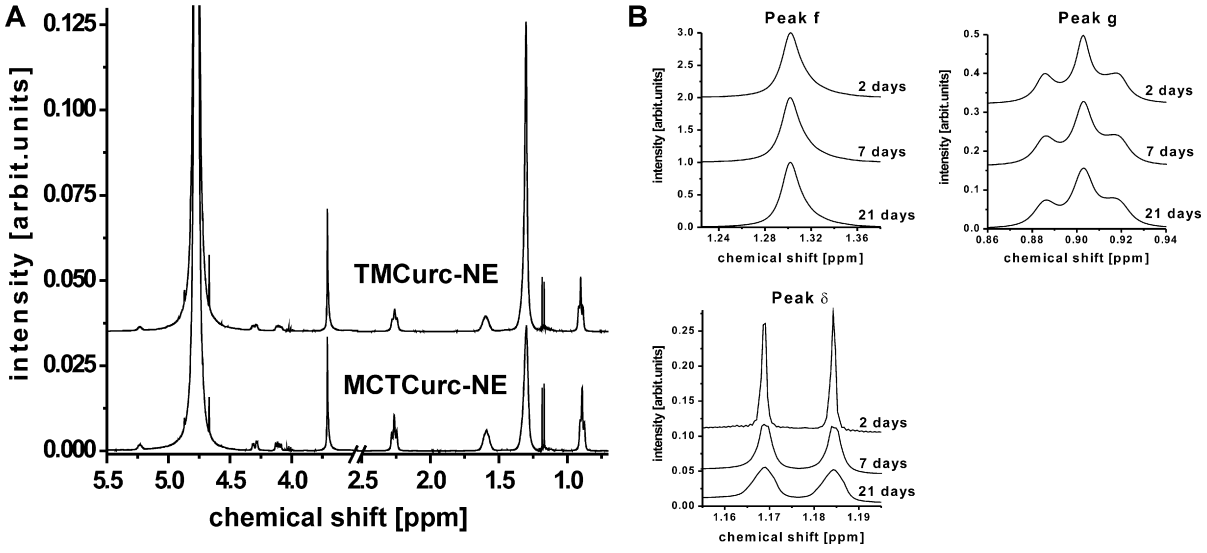

Fig. 8. (A) [1]H NMR spectra of a TMCurc-NE and a MCTCurc-NE dispersion. The spectra were recorded 48 h after production. The original spectra were normalized to the respective water signal (4.75 ppm). (B) [1]H NMR spectra of peak f, δ and peak g of a TMCurc-NE dispersion recorded 48 h, 7 days and 21 days after preparation and storage at 22 °C. The original spectra were normalized to peak f (1.3 ppm). The spectra were shifted along the ordinate for better visualization.

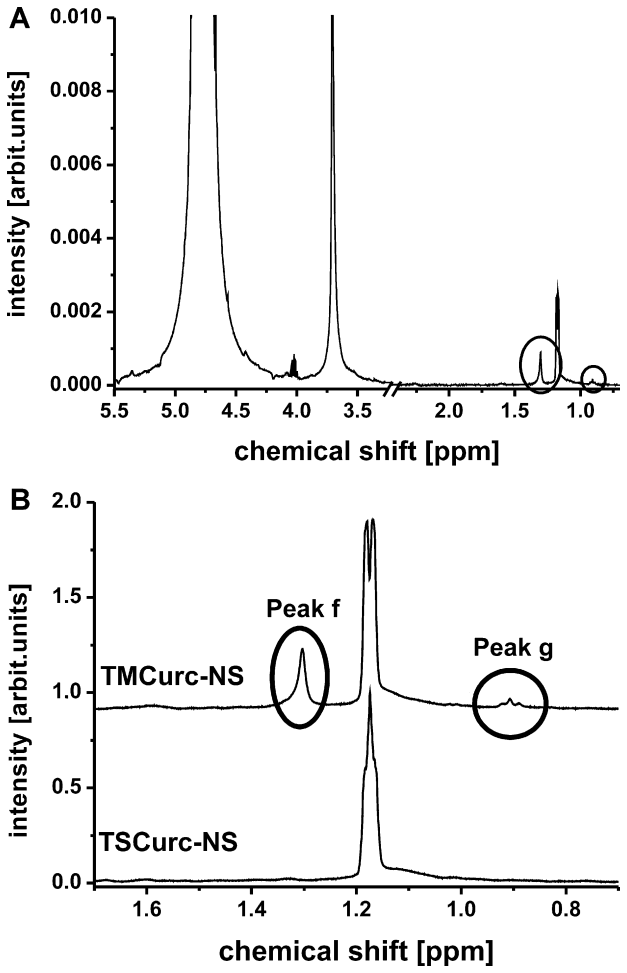

Fig. 9. (A) ^{1}H NMR spectrum of a TMCurc-NS dispersion recorded 48 h after production and storage at 8 °C. (B) ^{1}H NMR spectra of a TSCurc-NS and TMCurc-NS (enlargement of Fig. 9A) sample recorded 48 h after production and storage at 8 °C. The circles highlight the peaks f and g caused by protons of the triglyceride. The spectra were normalized and shifted along the ordinate for better visualization.

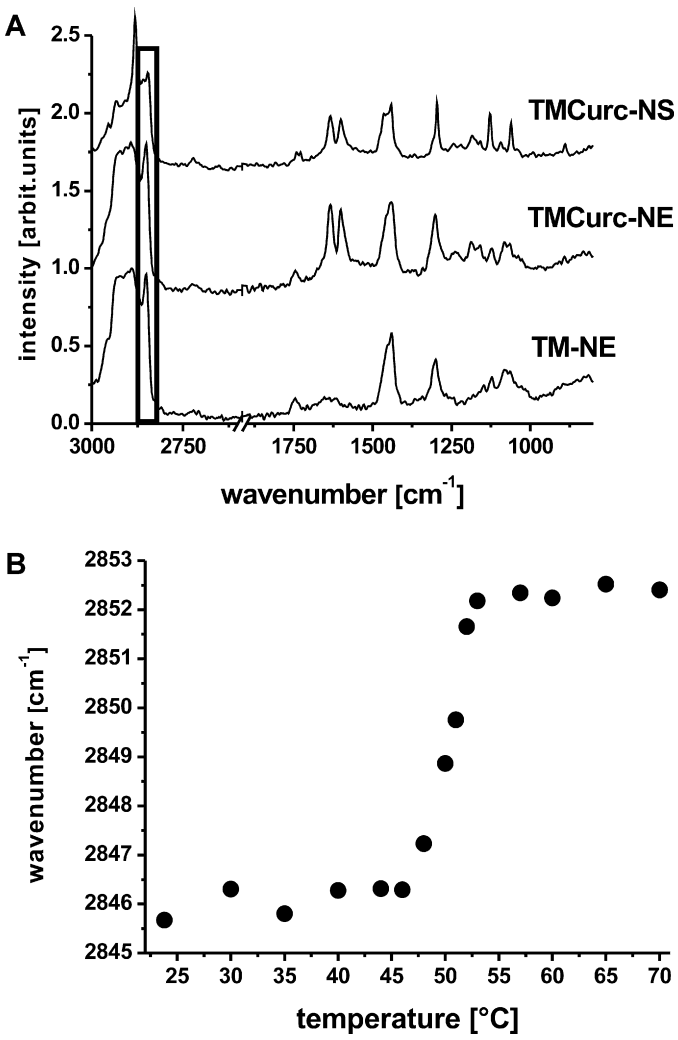

Fig. 10. (A) Raman spectra of a crystalline TMCurc-NS, a fluid TMCurc-NE and a drug-free fluid TM-NE preparation. The graphs were intercepted between 1900 cm^{-1} and 2600 cm^{-1}. The gray rectangle marks the symmetric CH_2-vibration (position ~2850 cm^{-1}). (B) Shift of the peak maximum of the symmetric CH_2-vibration during the continuous heating of a TMCurc-NS sample. The spectra were shifted along the ordinate for better visualization.

3.6. Raman spectroscopy

Among other information, the composition of the lipid, the physical state, the conformation of the lipid chain and the crystalline modification can be analyzed from the recorded Raman spectra. However, only few reports exist about an application of Raman spectroscopy for the characterization of colloidal lipid systems (Jores et al., 2005).

The recorded Raman spectra allowed a clear differentiation between the crystalline and the supercooled state of the TM nanoparticles (Fig. 10A). The crystalline matrix resulted in sharp peaks, whereas the peaks broadened in the liquid state.

The peak position of the symmetric CH_2-vibration of the fatty acid chain was used to monitor the melting of the solid nanoparticles (Fig. 10B). The rapid increase of the wavenumber at 50 °C was marking the melting event of the lipid. So the actual melting point found by Raman spectroscopy was somewhat lower compared to the values determined by DSC.

The spectra of the pure curcuminoids exhibited several sharp and intensive bands. The strongest were situated at 1601 cm^{-1} (phenol rings, peak a) and at 1630 cm^{-1} (CO—C=C, peak b) (Baranska et al., 2004). The recorded spectra showed a clear difference with respect to peak position and peak ratio between crystalline substance, curcuminoids amorphously embedded in Kollidon 12 PF and an ethanolic solution of the drug (Fig. 11A). Whereas the position of peak a was not changing, peak b was dependent on the physical state of the curcuminoids (Fig. 11A). Additionally, the intensity ratio peak a/peak b was bigger in the crystalline state compared to the dissolved curcuminoids (Fig. 11B). These characteristic changes were used to determine the state of the curcuminoids within the lipid nanodispersions.

The curcuminoid double band was well separated from the lipid signals (Fig. 10A). The signals of the incorporated curcuminoids were notably intensive, although the drug concentration in the preparation was at 0.1% (w/w). When the signals of the curcuminoids loaded onto the nanoparticles were compared to the spectra of the free curcuminoids it was assessed that they were more alike the spectrum of non-crystalline curcuminoids (Fig. 11A). The ratio peak a/peak b of the formulations was similar to the ratio of the amorphous embedding (Fig. 11B). Moreover, the curcuminoid ratio of the liquid and the solid nanoparticles were almost identical. Therefore, it was concluded that the major fraction of the drug remained in an amorphous or solubilized state when the formulation was cooled down after production. No substantial change in the physical condition of the drug when the lipid matrix was solidifying again. Mulik et al. (2010) suggested an amorphous state of the incorporated curcumin for their SLN preparation. The direct

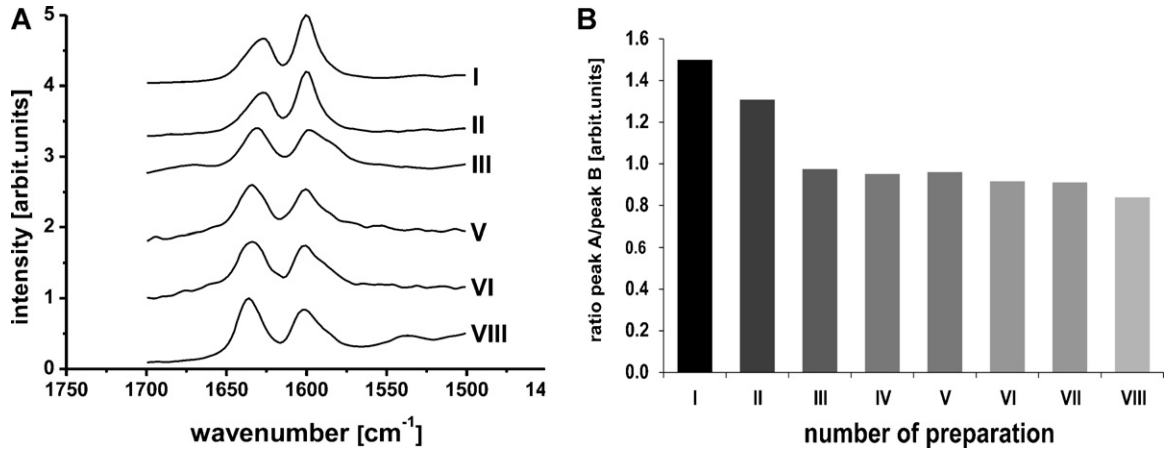

Fig. 11. (A) Raman spectra of the curcuminoid double band relative to the physical state of the drug. The spectra were shifted along the ordinate for better visualization. (B) Intensity ratio of the curcuminoid double band (peak a: 1600 cm^{-1}, peak b: 1633–1627 cm^{-1}) in different physical states. Investigated samples: (I) curcuminoid powder, (II) curcuminoid suspension [0.1% (w/v)], (III) curcuminoids embedded in Kollidon PF12 [0.1% (w/v)], (IV) TSCurc-NS (only Fig. 11B), (V) TMCurc-NS, (VI) TMCurc-NE, (VII) MCTCurc-NE (only Fig. 11B), (VIII) ethanolic solution of curcuminoids [0.2% (w/v)].

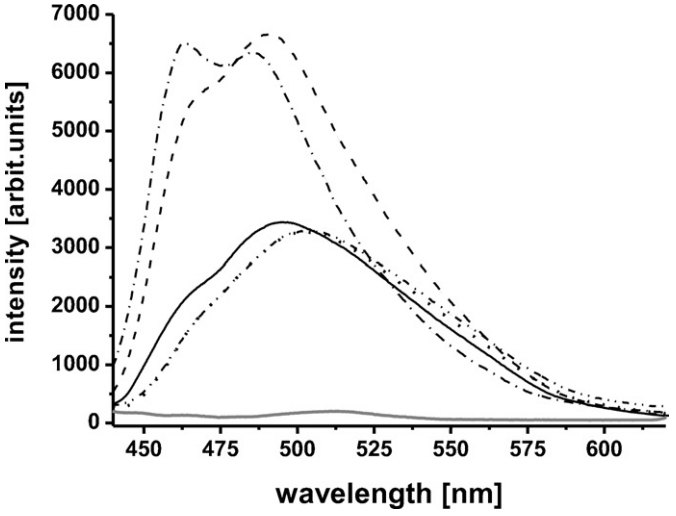

Fig. 12. Fluorescence spectra of the curcuminoids: dissolved in MCT (-·-·-) and in a MCTCurc-NE (- - -), TMCurc-NE (—), TMCurc-NS (···), TSCurc-NS, (-··-··-) or TM-NS (▬) dispersion. Curcuminoid concentration: 0.5 μg/ml in the MCT solution; 2.0 μg/ml in the nanodispersions.

incorporation of the curcuminoids into the highly ordered lipid matrix was rather improbable. The fate of the drug in the formulations was suggested to be as follows: (I) the curcuminoids are dissolved in the hot lipid, (II) the curcuminoids precipitate in the liquid droplets during cooling, (III) the lipid matrix recrystallizes and the curcuminoids are expulsed, (IVa) the drug is attached on the surface of the fully crystalline particles or (IVb) the curcuminoids are located in a solubilized state in the interface between water, emulsifier and solid lipid.

3.7. Fluorescence spectroscopy

The fluorescence spectrum of the curcuminoids in pure MCT showed an asymmetric peak with two maxima at 464 nm and 485 nm (Fig. 12). The spectra of the respective lipid nanodispersions were asymmetric, too, but their shape and position appeared to be very different from that of the bulk material. The maxima of MCTCurc-NE, TmCurc-NE, TMCurc-NS and TSCurc-NS were at 491 nm, 495 nm, 502 nm and 504 nm respectively (Fig. 12). No second maximum was detected in the nanodispersions, but a shoulder at higher wavelengths. This shoulder was expressed intensely in the spectrum of the MCTCurc-NE dispersion, got weaker for TMCurc-NE and could hardly be seen in the spectra of the crystalline nanoparticles.

The shift of the maximum indicated an increasing polarity in the environment of the curcuminoids. The red shift of curcumin dissolved in organic solvents with increasing polarity was reported before (Nardo et al., 2008; Khopde et al., 2009). In contrast to the apolar environment in bulk MCT, the curcuminoids will have more contact to polar regions within the emulsion droplets. Due to the small size of the droplets, a considerable part of the drug will also be situated at the interface between water and oil. The Raman data supported the idea that the curcuminoids were attached to the surface of the crystalline particles. Thus, the maxima would be shifted to higher wavelengths, because the majority of the drug was residing on the more polar surface of the particles. The structured shape of the different fluorescence spectra indicated the existence of several single species of the drug in the preparations. A fit with Gaussian functions was calculated to determine the number of single curves of which the recorded spectrum may be composed of. It was found that a stable fit was possible with four Gaussian functions. However, an assignment of the gathered fitting curves to a certain state of the curcuminoids was not possible. One reason for the special shape of the spectra could be the keto–enol tautomerism of the curcuminoids. It was reported that this phenomenon causes structured bands in the spectrum of curcuminoids dissolved in aprotic, non-polar, organic solvents (Nardo et al., 2008). However, possible regions of different polarities within the particles can be seen as another reason for the multimodal shape of the spectrum. In addition, scattered light from the particles may also influence the aspect of the fluorescence peak, although the light scattering of an unloaded TM-NE preparation was only weak (Fig. 12). The fluorescence intensity of the curcuminoids was much lower when they were incorporated in the lipid nanoparticles compared to the MCT solution. The ratio of the fluorescence intensity to the concentration of the curcuminoids was determined. The lowest ratio was calculated for the crystalline TMCurc-NS and TSCurc-NS preparations. This value was related to the ratios of the other formulations. Compared to the crystalline nanoparticles, the fluorescence/concentration ratio was almost equal for TMCurc-NE, but four times higher for MCTCurc-NE and eight times higher for the MCT solution of the curcuminoids. Therefore, the fluorescence intensity of the curcuminoids was dependent on the kind of lipid phase and on the dispersity of this phase. The reduced curcuminoid

fluorescence of the nanoparticles was explained by the quenching effect of water. It was reported by Jasim et al. that the presence of water effectively quenched the fluorescence of curcuminoids. The authors postulated that the water molecule and the fluorescent dye build a complex which is not fluorescent (Jasim and Ali, 1992). Due to the big surface of the nanoparticles, an intense interaction of the drug in the particle and the surrounding water was possible. The smaller intensity of the crystalline dispersions was caused by the presence of the majority of the curcuminoids on the surface of the particles where they were distinctly quenched by the present water. In contrast, the curcuminoids were allowed to diffuse freely within the oil droplets of the emulsion which reduced the quenching effect. However, the different fluorescence intensities of TMCurc-NE and MCTCurc-NE cannot be explained by the quenching effect of water. The different solubilities of the curcuminoids in the respective lipid may be the basic reason for the differences between the two emulsions. The curcuminoids were dissolved under constant heating in the respective lipid before homogenization. It was found that the drug was dissolved better in MCT compared to TM or TS. Curcuminoids may have precipitated, in part, within the emulsion droplets, during the cooling step after preparation. The non-dissolved fraction exhibited a less intense fluorescence compared to the dissolved curcuminoids. The fraction of dissolved curcuminoids is thought to be bigger in MCTCurc-NE, resulting in a higher fluorescence intensity. Conclusively, the fluorescence of the curcuminoids is among others influenced by the quenching effect of water and by its solubility in the respective lipid phase.

The heating and subsequent melting of a sample of TMCurc-NS had a big impact on the fluorescence properties of the incorporated drug (Fig. 13). The melting process influenced the maximum intensity, the peak position and the shape of the peak. The higher mobility and bigger thermal energy of the surrounding water caused an increased quenching at higher temperatures resulting in a smaller I_{max} of the spectrum (Fig. 13B). This phenomenon was also seen when MCTCurc-NE or TMCurc-NE were continuously heated. In these preparations the increasing temperature of the lipid in the droplets was seen as the main cause for the curcuminoid quenching and the surrounding water played only a minor role. The red shift of the fluorescence spectrum of TMCurc-NS pointed to an increased polarity of the environment of the drug. This was explained by a better penetration of the water molecules onto the surface of the particles with rising temperature. At around 48 °C the fluorescence intensity of the TMCurc-NS sample was slightly increasing and the peak position was shifting to smaller wavelength (Fig. 13A). This marked the beginning of the melting process. The maximum intensity and minimum peak position was reached at 51 °C (Fig. 13B). At that point the lipid matrix was completely molten. The melting temperature was a bit lower compared to the temperature found by DSC, but coincided well with the temperature-dependent Raman measurements (see Section 3.5). Above 51 °C, the intensity fell again and the peak maximum was shifted to higher wavelength. Besides the changes of fluorescence intensity and peak position, the shape of the spectrum was changing, too. The shoulder at higher wavelengths, typically found for liquid lipids, was appearing at 49 °C indicating a liquid fraction within the nanoparticles. The blue shift of the peak during the melting process was caused by a decreasing polarity, because the curcuminoids could diffuse from the surface of the particles in the liquid center. The increasing fluorescence intensity was possibly caused by a partly solubilization of the curcuminoids in the lipid matrix.

The fluorescence anisotropy of the curcuminoids in the applied solvents and in the nanoparticles was clearly different (Fig. 14). Pure MCT had the highest anisotropy values, which proved that the curcuminoids are highly immobile within the oil. In contrast, the anisotropy was only low for a solution of curcuminoids in

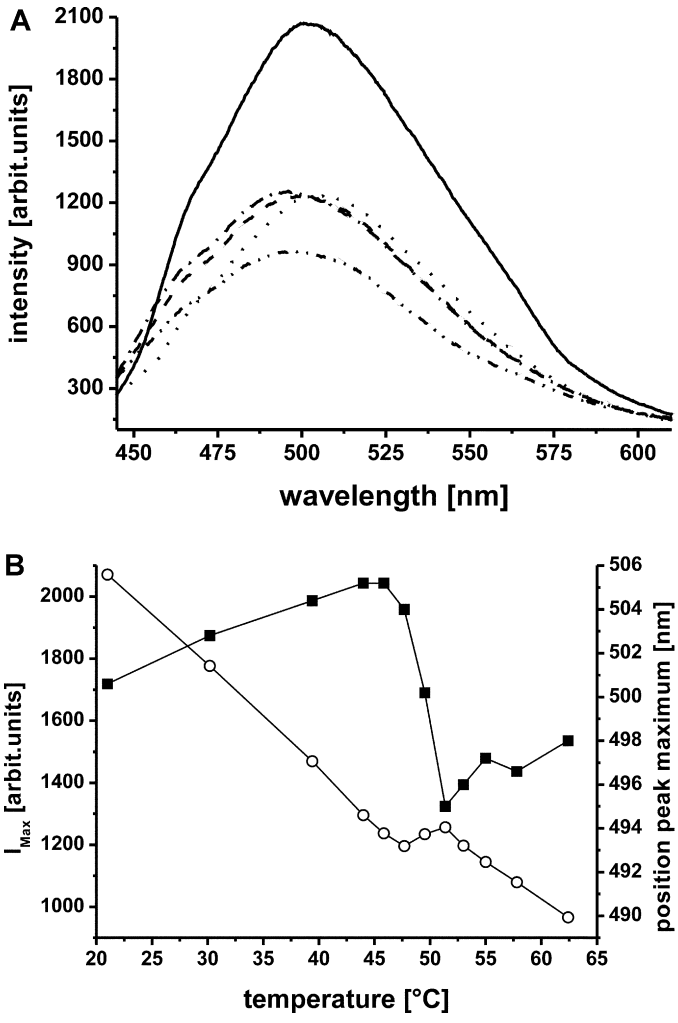

Fig. 13. (A) Fluorescence spectra of a TMCurc-NS dispersion at 21 °C (—), 46 °C (···), 49 °C (- - -), 51 °C (-·-·) and 62 °C (-··-··-). Curcuminoid concentration: 2 μg/ml. (B) Maximum intensity (–○–) and peak maximum (–■–) of the fluorescence spectra of a TMCurc-NS preparation during continuous heating.

acetone and the mobility of the drug appeared to be high within the organic solvent. The curcuminoid-loaded dispersions exhibited anisotropies of around 0.2 and were situated between acetone and MCT. The obtained results were explicitly lower compared

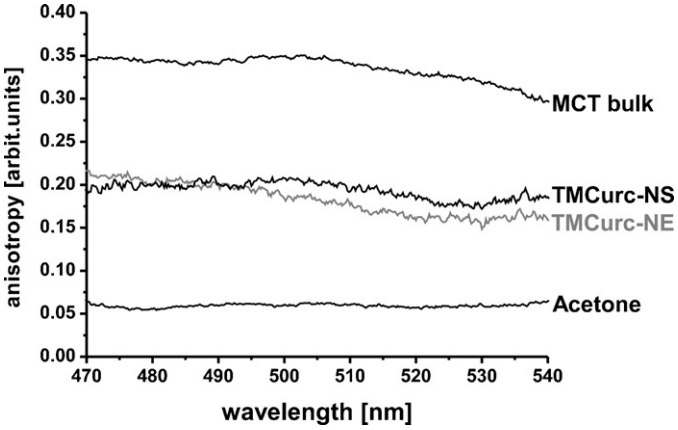

Fig. 14. Fluorescence anisotropy of curcuminoids: dissolved in MCT (1 μg/ml), in a TMCurc-NS preparation (2 μg/ml), in a TMCurc-NE (2 μg/ml) preparation and dissolved in acetone (1 μg/ml).

to the anisotropy of curcumin associated to proteins or phospholipid micelles (Began et al., 1999; Kapoor and Priyadarsini, 2001; Barik et al., 2003). Thus, the curcuminoids were still maintaining a considerable mobility within the nanoparticles. Interestingly, no clear difference in anisotropy between fluid and solid matrix was detectable. Hence, it is suggested that the curcuminoids are not adhered strongly on the lipid surface of the crystalline particles, but are rather enclosed loosely in the particles. With regard to drug-loading the solid lipid nanoparticles were therefore not a static system. On the contrary, the environment, e.g. polarity, temperature, ionic strength had a severe impact on the properties of the curcuminoids severely.

4. Conclusion

Three different formulations of curcuminoid-loaded lipid nanodispersions were successfully produced and their properties were investigated. All preparations had a mean particle size below 170 nm. The dispersions were not showing any fractions >1 μm when examined under a light microscope. The TEM micrographs displayed an irregular shape of the solid lipid particles. The supercooled state of the TM dispersions was demonstrated by the DSC, ^{1}H NMR and Raman measurements. The drug-free preparations remained in the metastable state for the whole observation period, whereas the curcuminoid-loaded dispersions were partially recrystallizing. When the TM dispersions were cooled down they were solely crystallizing in the stable β-modification. In contrast, the TS dispersions partially contained α-modified lipid beside a large lipid fraction of β-modification. The α-modified lipid was subsequently converted into β-modification within 16 weeks. The ^{1}H NMR investigations showed that the mobility of the liquid lipid phase of TMCurc-NE was not changing over a period of 3 weeks. The signals of the emulsifier were broadening over time which was explained with a further ordering of the polymer chains in the lipid dispersions. In TMCurc-NS, a fraction of free fatty acids and partial glycerides was detected by ^{1}H NMR. Raman spectroscopy gave unique information about the localization of the curcuminoids within the particle and their physical state. It was demonstrated that the ratio of the double band at 1600 cm^{-1} was depending on the physical state of the curcuminoids. The curcuminoid bands of the drug-loaded dispersions were similar in shape and ratio to the non-crystalline free substance. It was concluded that the curcuminoids were enclosed in an amorphous state within the particles. Our data suggested that the application of this method can help to elucidate the interaction of drug and lipid matrix, even at low concentrations of the drug. Further details of the drug–carrier interaction were gained by fluorescence spectroscopy. The shape and position of the fluorescence peak was influenced by the lipid matrix. The curcuminoids incorporated in the crystalline particles exhibited a red shift of the spectrum, which indicated that the drug was situated in a more polar environment. The continuous heating of the nanodispersions demonstrated that the surrounding environment had an influence on the properties of the curcuminoids. It was shown that the nanoparticles were not a separated system, but interacting with the surrounding media. The melting of the lipid phase had a direct impact on the fluorescence properties of the curcuminoids. From the results of the fluorescence and the Raman measurements it was concluded that the curcuminoids were separated from the lipid matrix during crystallization and were attached to the surface of the particles. The mobility of the curcuminoids within the nanoparticles was decreased compared to a solution of the drug in an organic solvent, but still higher than in an oily solution. Thus, the conditions within the particles are fairly different from that in the lipid bulk material.

Acknowledgments

The authors thank Günter Förster (Institute of Physical Chemistry, MLU Halle-Wittenberg) for the support with the X-ray scattering measurements, Kerstin Schwarz (Institute of Pharmacy, MLU Halle-Wittenberg) for the DSC measurements, Heike Rudolf (Institute of Pharmacy, MLU Halle-Wittenberg) for the Raman measurements, Hans-Herrmann Rüttinger (Institute of Pharmacy, MLU Halle-Wittenberg) for the support with the fluorescence spectroscopy measurements and Dieter Ströhl (Institute of Organic Chemistry, MLU Halle-Wittenberg) for the ^{1}H NMR measurements.

References

Aggarwal, B.B., Harikumar, K.B., 2009. Potential therapeutic effects of curcumin, the anti-inflammatory agent, against neurodegenerative, cardiovascular, pulmonary, metabolic, autoimmune and neoplastic diseases. Int. J. Biochem. Cell Biol. 41, 40–59.

Aggarwal, B.B., Ichikawa, H., Garodia, P., Weerasinghe, P., Sethi, G., Bhatt, I.D., Pandey, M.K., Shishodia, S., Nair, M.G., 2006. From traditional Ayurvedic medicine to modern medicine: identification of therapeutic targets for suppression of inflammation and cancer. Expert Opin. Ther. Targets 10, 87–118.

Al-Saden, A.A., Whateley, T.L., Florence, A.T., 1982. Poloxamer association in aqueous solution. J. Colloid Interface Sci. 90, 303–309.

Anand, P., Kunnumakkara, A.B., Newman, R.A., Aggarwal, B.B., 2007. Bioavailability of curcumin: problems and promises. Mol. Pharm. 4, 807–818.

Anand, P., Sundaram, C., Jhurani, S., Kunnumakkara, A.B., Aggarwal, B.B., 2008a. Curcumin and cancer: an old-age disease with an age-old solution. Cancer Lett. 267, 133–164.

Anand, P., Thomas, S.G., Kunnumakkara, A.B., Sundaram, C., Harikumar, K.B., Sung, B., Tharakan, S.T., Misra, K., Priyadarsini, I.K., Rajasekharan, K.N., Aggarwal, B.B., 2008b. Biological activities of curcumin and its analogues (Congeners) made by man and Mother Nature. Biochem. Pharmacol. 76, 1590–1611.

Baranska, M., Schulz, H., Rosch, P., Strehle, M.A., Popp, J., 2004. Identification of secondary metabolites in medicinal and spice plants by NIR-FT-Raman microspectroscopic mapping. Analyst 129, 926–930.

Barik, A., Priyadarsini, K.I., Mohan, H., 2003. Photophysical studies on binding of curcumin to bovine serum albumin. Photochem. Photobiol. 77, 597–603.

Began, G., Sudharshan, E., Udaya Sankar, K., Ppu Rao, A.G., 1999. Interaction of curcumin with phosphatidylcholine: a spectrofluorometric study. J. Agric. Food Chem. 47, 4992–4997.

Blümer, C., Mäder, K., 2005. Isostatic ultra-high-pressure effects on supercooled melts in colloidal triglyceride dispersions. Pharm. Res. 22, 1708–1715.

Bunjes, H., Koch, M.H.J., Westesen, K., 2000. Effect of particle size on colloidal solid triglycerides. Langmuir 16, 5234–5241.

Bunjes, H., Koch, M.H.J., Westesen, K., 2003. Influence of emulsifiers on the crystallization of solid lipid nanoparticles. J. Pharm. Sci. 92, 1509–1520.

Bunjes, H., Steiniger, F., Richter, W., 2007. Visualizing the structure of triglyceride nanoparticles in different crystal modifications. Langmuir 23, 4005–4011.

Bunjes, H., Westesen, K., Koch, M.H.J., 1996. Crystallization tendency and polymorphic transitions in triglyceride nanoparticles. Int. J. Pharm. 129, 159–173.

Duvoix, A., Blasius, R., Delhalle, S., Schnekenburger, M., Morceau, F., Henry, E., Dicato, M., Diederich, M., 2005. Chemopreventive and therapeutic effects of curcumin. Cancer Lett. 223, 181–190.

Förster, G., Schwieger, C., Faber, F., Weber, T., Blume, A., 2007. Influence of poly(L-lysine) on the structure of dipalmitoylphosphatidylglycerol/water dispersions studied by X-ray scattering. Eur. Biophys. J. 36, 425–435.

Jasim, F., Ali, F., 1992. A novel and rapid method for the spectrofluorometric determination of curcumin in curcumin spices and flavors. Microchem. J. 46, 209–214.

Jores, K., Haberland, A., Wartewig, S., Mäder, K., Mehnert, W., 2005. Solid lipid nanoparticles (SLN) and oil-loaded SLN studied by spectrofluorometry and Raman spectroscopy. Pharm. Res. 22, 1887–1897.

Jores, K., Mehnert, W., Mäder, K., 2003. Physicochemical investigations on solid lipid nanoparticles and on oil-loaded solid lipid nanoparticles: a nuclear magnetic resonance and electron spin resonance study. Pharm. Res. 20, 1274–1283.

Kapoor, S., Priyadarsini, K.I., 2001. Protection of radiation-induced protein damage by curcumin. Biophys. Chem. 92, 119–126.

Khopde, S.M., Indira Priyadarsini, K., Dipak, K., Mukherjee, T., 2009. Effect of solvent on the excited-state photophysical properties of curcumin. Photochem. Photobiol. 72, 625–631.

Kuntsche, J., Klaus, K., Steiniger, F., 2009. Size determinations of colloidal fat emulsions: a comparative study. J. Biomed. Nanotechnol. 5, 384–395.

Kuntsche, J., Westesen, K., Drechsler, M., Koch, M.H.J., Bunjes, H., 2004. Supercooled smectic nanoparticles: a potential novel carrier system for poorly water soluble drugs. Pharm. Res. 21, 1834–1843.

Lakowicz, J.R., Masters, B.R., 2008. Principles of fluorescence spectroscopy. J. Biomed. Opt. 13, 029901.

Lao, C.D., Ruffin, M.T., Normolle, D., Heath, D.D., Murray, S.I., Bailey, J.M., Boggs, M.E., Crowell, J., Rock, C.L., Brenner, D.E., 2006. Dose escalation of a curcuminoid formulation. BMC Complement. Altern. Med. 6, 10.

Lutton, E.S., 1945. The polymorphism of tristearin and some of its homologs. J. Am. Chem. Soc. 67, 524–527.

Mehnert, W., Mäder, K., 2001. Solid lipid nanoparticles: production, characterization and applications. Adv. Drug Deliv. Rev. 47, 165–196.
Mulik, R.S., Mönkkönen, J., Juvonen, R.O., Mahadik, K.R., Paradkar, A.R., 2010. Transferrin mediated solid lipid nanoparticles containing curcumin: enhanced in vitro anticancer activity by induction of apoptosis. Int. J. Pharm. 398, 190–203.
Müller, R.H., Mehnert, W., Lucks, J.S., Schwarz, C., Zur Mühlen, A., Meyhers, H., Freitas, C., Rühl, D., 1995. Solid lipid nanoparticles (SLN): an alternative colloidal carrier system for controlled drug delivery. Eur. J. Pharm. Biopharm. 41, 62–69.
Nardo, L., Paderno, R., Andreoni, A., Másson, M., Haukvik, T., Tønnesen, H.H., 2008. Role of H-bond formation in the photoreactivity of curcumin. Spectroscopy 22, 187–198.
Nobbmann, U., Morfesis, A., 2009. Light scattering and nanoparticles. Mater. Today 12, 52–54.
Priano, L., Esposti, D., Esposti, R., Castagna, G., De Medici, C., Fraschini, F., Gasco, M.R., Mauro, A., 2007. Solid lipid nanoparticles incorporating melatonin as new model for sustained oral and transdermal delivery systems. J. Nanosci. Nanotechnol. 7, 3596–3601.
Small, D.M., Hanahan, D.J., 1986. The Physical Chemistry of Lipids: From Alkanes to Phospholipids. Plenum press, New York.
Strimpakos, A.S., Sharma, R.A., 2008. Curcumin: preventive and therapeutic properties in laboratory studies and clinical trials. Antioxid. Redox Signal. 10, 511–545.
Tuli Jr., R., Surmak, A., Herman, J.M., 2011. Effect of diferuloyl methane (curcumin) on radiation-induced inhibition of proliferation and cytotoxicity of pancreatic cancer cells. J. Clin. Oncol. 29, 222.
Westesen, K., Bunjes, H., 1995. Do nanoparticles prepared from lipids solid at room temperature always possess a solid lipid matrix? Int. J. Pharm. 115, 129–131.
Yang, S., Zhu, J., Lu, Y., Liang, B., Yang, C., 1999. Body distribution of camptothecin solid lipid nanoparticles after oral administration. Pharm. Res. 16, 751–757.
Youssef, K.M., El-Sherbeny, M.A., 2005. Synthesis and antitumor activity of some curcumin analogs. Arch. Pharm. 338, 181–189.
Zhong, F., Chen, H., Han, L., Jin, Y., Wang, W., 2011. Curcumin attenuates lipopolysaccharide-induced renal inflammation. Biol. Pharm. Bull. 34, 226–232.